RSC Applied Interfaces

ROYAL SOCIETY OF CHEMISTRY

PAPER

View Article Online
View Journal | View Issue

Cite this: *RSC Appl. Interfaces*, 2025, **2**, 1799

Novel Ca–Ti-modified alkali-activated metakaolin adsorbent: multimetal adsorption and regeneration mechanisms

M. Korhonen, A. T. Pikkarainen, T. Hu, V. Srivastava, H. Runtti, S. Tuomikoski and U. Lassi *

Adsorbents such as activated carbon and ion exchange resins have several limitations, including high operational and regeneration costs. These drawbacks have prompted the search for alternative adsorbent materials that offer benefits such as cost-effectiveness, chemical stability, safe regenerability, and minimal waste generation. Alkali-activated materials (AAMs) have emerged as a promising solution, especially when engineered into larger forms—such as casted columns—*via* alkali-activation manufacturing. This approach not only broadens their applicability across various processes but also enhances surface area and porosity, thereby improving adsorption performance. In this study, titanate-modified metakaolin was cast into a column, achieving multimetal adsorption capacities of 13.4, 32.3, 43.3, 49.0, 52.8, 54.0, 61.8, and 66.6 mg g^{-1} for Li, Ni, Co, Zn, Mn, Cu, Cd and Pb, respectively. The regeneration ability of AAM adsorbent was demonstrated through 31 consecutive adsorption–desorption cycles. A novel regeneration chemical, 0.5 M citric acid (pH 6.6), exhibited exceptional regeneration potential without compromising the mechanical strength of the AAM—an issue commonly encountered with other regeneration chemicals. The removal efficiency remained above 95% throughout all cycles, indicating only a 4% reduction in adsorption performance. Both adsorption and regeneration mechanisms were proposed in this study. The AAM was characterized using X-ray diffraction (XRD), X-ray spectroscopy (XPS), X-ray fluorescence (XRF), field emission scanning electron microscopy with energy-dispersive X-ray spectrometry (FESEM-EDS), and diffuse reflectance infrared Fourier transform spectroscopy (DRIFTS). The sustainability and economic viewpoint of the process was studied through a life-cycle assessment (LCA) method.

Received 26th June 2025,
Accepted 31st August 2025

DOI: 10.1039/d5lf00184f

rsc.li/RSCApplInter

Introduction

Hazardous or toxic pollutants are a major threat to both the environment and health. Even trace amounts of heavy metals can cause severe health issues and can even be categorized as carcinogenic. Industrial wastewater commonly contains harmful pollutants, such as copper, zinc, and manganese.[1–4] These heavy metals enter the water systems usually through industrial activities such as mining and metal refining. To protect aquatic ecosystems, there are regulations that wastewater must be purified with effective methods and materials to minimize the environmental impact.[2,5]

Different methods are used in water purification, such as ion exchange, membrane filtration, precipitation, and adsorption. Adsorption is an inexpensive, easy, and widely applied method in mining, chemical, steel, pulp, paper, dairy, and textile industries. Moreover, the adsorption process facilitates the recovery of critical earth metals, contributing to resource circularity and reducing reliance on foreign supply chains.[1,2,6]

Activated carbon remains one of the most widely used commercial adsorbents. However, alternative materials such as alkali-activated materials (AAMs), derived from inorganic raw materials, are gaining attention due to their cost-effectiveness and proven efficiency in removing metals from wastewater.[4,7] AAMs can also be synthetized from industrial by-products like slags,[4,8,9] promoting waste valorization and enhancing their appeal for industrial applications. Additionally, AAMs show promising potential for reuse, with the ability to undergo multiple adsorption–regeneration cycles.[2,9] Nonetheless, their performance typically declines after fewer than five cycles due to reduced adsorption capacity.[10–12]

Titanosilicates and titanate-based adsorbents/catalysts have turned out to have excellent efficacy in removing radioactive and rare earth metals from waste streams.[13–23] In this study, a new AAM was created by doping metakaolin with calcium titanate to obtain a mechanically strong adsorbent to ameliorate adsorption efficacy, which is suitable for concentrated wastewater containing heavy metals. The material was cast

Research Unit of Sustainable Chemistry, University of Oulu, P.O. Box: 4300, FI-90014, Oulu, Finland. E-mail: ulla.lassi@oulu.fi

directly to the column to enhance the porosity and surface area. Adsorption and regeneration processes were optimized in relation to concentration, pH and time. To prove reusability, 31 adsorption regeneration cycles were conducted with a newly developed regeneration chemical. A 99.85% of the adsorption capacity recovery average was achieved after every cycle. The AAM was characterized by X-ray diffraction (XRD), X-ray fluorescence (XRF), X-ray photoelectron spectroscopy (XPS), field emission scanning electron microscopy with energy-dispersive X-ray spectrometry (FESEM-EDS), and diffuse reflectance infrared Fourier-transform spectroscopy (DRIFTS). In addition, life-cycle assessment was done to determine the sustainability of the full process. The novelty of this study lies in the development of a wasteless adsorption process utilizing an abundant alkali-activated metakaolin adsorbent, which demonstrates exceptionally high multimetal recovery rates (>99%) and outstanding regenerability. To the best of our knowledge, such recovery efficiencies and regeneration performance have not been previously reported for similar types of adsorbents. Additionally, the adsorbent was used in column form without any supporting structure, further simplifying the system and enhancing its practical applicability.

Materials and methods

Reagents

Alkali solutions were prepared from sodium hydroxide (NaOH; AnalR NORMAPUR, VWR Chemicals, Czech Republic) mixed with sodium silicate solution (Na_2SiO_3, extra pure; Supelco®, Merck KGaA, Germany). The Na_2SiO_3 solution consisted of 27% SiO_2, 8.0% Na_2O, and 65% H_2O. Virgin olive oil (extra virgin cold pressed, Borges, Spain) was used as a surfactant and 3% hydrogen peroxide (H_2O_2; 30% (w/v), AnalR NORMAPUR, VWR Chemicals, France) was used as a foaming agent (porogen). Washed white kaolin (VWR Chemicals, Belgium) was used to produce metakaolin (*i.e.*, calcined kaolin). Calcium titanate was acquired from Thermo Scientific (99+%, Thermo Scientific, Germany).

Synthesis of adsorbent material

An alkali solution was prepared by mixing for 2 hours with a magnetic stirrer at 300 rpm a solution of sodium silicate (45.05%) comprising 27.0% SiO_2, 8.0% Na_2O and 65% H_2O in wt%, and granular sodium hydroxide (6.88%) covered by a watch glass to prevent water evaporation. The solution was aerated with a homogenizer (OV5, Velp Scientifica srl, Italy) with rotor attachment (VCR2, Velp Scientifica, Italy) for 30 seconds with a speed of 20 000 rpm. A mixture of metakaolin (27.57%) and calcium titanate ($CaTiO_3$, 9.19%) was added by mixing with an IKA RW 20 digital overhead stirrer (IKA® Werke GmbH & Co. KG, Germany) with an R 1382 three-bladed propeller stirrer (IKA® Werke GmbH & Co. KG, Germany) to the aerated alkali solution in 5 minutes with a mixing speed of 1200 rpm to solubilize the metals of the metakaolin and calcium titanate to the alkali solution. The metakaolin was prepared by heating calcined kaolin in a ceramic oven (Model L5/11/P320; Nabertherm GmbH, Germany) from 25 °C to 750 °C with 5 °C min^{-1} increment, maintaining at 750 °C for 3 hours, and decreasing the temperature from 750 °C to 25 °C with 5 °C min^{-1} decrease. The mass loss during calcination was 12.5%.

Extra virgin olive oil (5.52%) comprising saturated fatty acids (*i.e.*, triglycerides) was added to the mass by mixing at 1200 rpm for 10 minutes as a surfactant. Triglycerides react under alkaline conditions, such as in a strong base or sodium or potassium hydroxide, to produce glycerol and fatty acid salts (soap).[24] This process is called saponification. Furthermore, glycerol formed from the reaction is further degraded to release hydrogen to the mass, increasing the porosity. At the end of the mixing period, 5.79% dilute hydrogen peroxide (1.38% (30% H_2O_2) + 4.41% H_2O) is added by mixing at 500 rpm for 5 minutes to obtain the optimal porosity while maintaining the correct water content allowing the metals to migrate during polymerization. The obtained mass was poured into a column (about 40% of the column volume), placed in an airtight container and cured in an oven (Type TS 8056, Termaks, Bergen, Norway) at 67 °C for 48 hours. The airtight container maintained the moisture inside the column which was released after 24 hours to speed up the drying. During the drying the volume of the mass expanded by about 250% and the mass was cured by a polymerization reaction, which cross-links the materials into a metal network by oxygen bridging.

After drying, in the case of the column, the excess material was removed. Excess glycerol was washed from the materials with 75 °C water with flow-through until the pH of the washing water was 8.5. After regeneration with sodium citrate solution, the Ti-doped AAM adsorption column was ready for use. When moulded into a column, the adsorption area increases, as the sample to be treated flows through the whole column material, which is opposite to powdery or granular adsorbent, wherein the adsorption occurs only at the surface of the object.

Characterization methods of AAM

The crystalline phase of the AAM sample was determined *via* the XRD method (PANalytical X'Pert Pro, Almelo, the Netherlands) using monochromatic Cu Kα1 radiation (λ = 1.5406 Å) at 45 kV and 40 mA with a scan step size of 0.017° and 2θ of 8–85°. The diffractograms were analyzed using X'Pert Highscore (PANalytical B.V., the Netherlands) and compared with the Powder Diffraction File standards from the International Centre for Diffraction Data (ICDD, PDF-4+ 2024).

The composition of metal oxides in the prepared AAM was determined using an XRF spectrometer (PANalytical Axios mAX XRF, Almelo, the Netherlands). The measurements were performed using loose powders run through transparent Mylar films under a He atmosphere.

DRIFTS was used to investigate the degree of polymerization in the prepared sample. DRIFTS spectra were recorded on a

Bruker PMA 50 Vertex 80 V (Bruker, Billerica, MA, USA) equipped with a Harrick Praying Mantis™ diffuse reflection accessory for baseline measurement using KBr. Measurements were conducted at 400–4000 cm^{-1} with a resolution of 4 cm^{-1} and 500 scans per min.

The microstructure and morphology of the samples were investigated using a Zeiss Sigma FESEM (Carl Zeiss Microscopy GmbH, Jena, Germany). The FESEM images were taken at 5 kV at magnifications ranging from 150 to 100k.

XPS analysis was performed using an ESCALAB 250Xi XPS System (Thermo Fisher Scientific, Waltham, MA, USA). The sample was placed into a gold sample holder, and a high-resolution scan was conducted with a pass energy of 20 eV. The pass energy for a survey scan was 150 eV. The monochromatic Al Kα radiation (1486.7 eV) was operated at 20 mA and 15 kV with an X-ray spot size of 900 μm. Oxygen, calcium, silica, magnesium, and carbon were measured, and the data were analyzed using the Avantage V5 program. Charge compensation was performed by applying the C 1s peak at 284.8 eV as a reference. XRD, XRF, FESEM, and XPS facilities were used at the Centre for Material Analysis, University of Oulu, Finland.

Liquid samples from adsorption and regeneration experiments were analyzed using flame atomic absorption spectroscopy (AAS, Varian AA240FS; Varian Inc., Palo Alto, CA, USA) with a Cu–Fe–Mn–Zn HC lamp (Agilent Technologies, Australia) and inductively coupled plasma optical emission spectrometry (ICP-OES, Agilent 5110 VDV, Agilent Technologies, USA) with nebulizer, plasma and auxiliary flows of 0.7, 12.0 and 1.0 L min^{-1}, respectively.

Adsorption experiments

AAM was studied as an adsorbent material for different pollutants: Zn, Cu, Mn, Ni, Co, Pb, Cd and Li. Adsorption experiments were performed in two different column sizes: column a (diameter 4 cm, height 10 cm) and column b (diameter 9 cm, height 7.86 cm), giving a total volume of 0.126 L for column a and 0.5 L for column b. After the experiments, the columns were dismantled, and the adsorbent was dried in an oven at 105 °C and weighed to calculate the q-values. The mass of the adsorbents was 27.01 g for column a and 137.23 g for column b.

The adsorbate solution was directed upstream through the column. The AAM column was treated with a solution of $ZnCl_2$, $CuSO_4$, $MnSO_4$, $NiSO_4$, $CoCl_2$, $PbC_4H_6O_4$, $CdCl_2$ and LiCl with a calculated content of cations. Two different flow configurations were used, closed loop and direct flow (Fig. 1). In closed loop, the permeate was directed back to the sample beaker. Due to the permeate's higher pH (pH 6), 0.1 M HCl was added to the sample vessel to maintain a constant pH value of 4.5. In adsorption experiments, concentrations (100–5000 mg L^{-1}) and flow rates (50–250 mL min^{-1}) at a constant pH of 4.5 were studied. The temperature was kept constant at room temperature (25 °C). All the samples, including the blank sample, were filtered through a 0.45 μm polyethersulfone (PES) syringe filter (33 mm syringe filter, sterile, Thermo Fisher Scientific) to avoid hydroxide precipitation affecting the results.

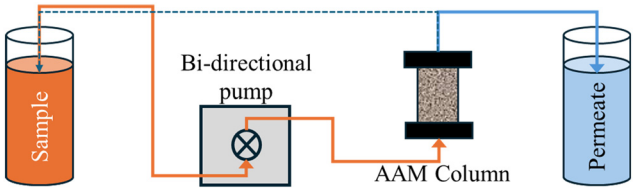

Fig. 1 Setup for column experiments. The dotted line presents a "closed loop" setup and the solid line is normal, direct flow setup.

Adsorption/desorption of cations was assumed to be a reversible mechanism:

$$Me^{z+}_{(aq)} \leftrightarrow Me^{z+}_{(s)} \quad (1)$$

where $Me^{z+}_{(aq)}$ is the hydrated cation in the sample solution and $Me^{z+}_{(s)}$ is the cation adsorbed on the surface of AAM.

Adsorption efficacy (q_{ads}) and removal percentage (R-%) were calculated as presented in eqn (2) and (3):

$$q_{ads} = \left(\frac{c_0 - c}{m}\right) \times V \quad (2)$$

$$R\text{-}\%(\text{adsorption}) = \frac{c_0 - c}{c_0} \times 100\% \quad (3)$$

where c_0 is the initial concentration (mg L^{-1}), c is the concentration after adsorption (mg L^{-1}), m is the adsorbent mass (g), and V is the volume of the adsorbate solution (L).[25,26]

Regeneration experiments

Regeneration was studied under different conditions to optimize the process in column type experiments completely. These experiments were done using AAM, which was first used in adsorption experiments. The flow direction in the column was downstream, which was in reverse compared to the adsorption process. The flow direction was changed to allow the pollutants to detach more easily, as they are more likely attached to the first possible adsorption site on the surface.[27] In the regeneration experiments, the pH of the regeneration solution (6.6–10.6) and the concentration of the regeneration solution (0.1–1 M) were optimized, while the temperature (25 °C) and flow rate (50 mL min^{-1}) were kept constant. Also, regeneration performance was investigated by conducting 31 adsorption–regeneration cycles with 500 mg L^{-1} copper solution.

Regeneration efficacy (q_{reg}) and removal percentage (R-%) were calculated as presented in eqn (4) and (5).

$$q_{reg} = \left(\frac{c}{m}\right) \times V \quad (4)$$

$$R\text{-}\%(\text{regeneration}) = \frac{q_{reg}}{q_{ads}} \times 100\% \quad (5)$$

where c is the metal concentration in the regeneration solution after regeneration (mg L^{-1}), m is the adsorbent mass (g), and V is the volume of the regeneration solution (L).[26,28,29]

LCA

A life cycle assessment (LCA) tool is usually employed to determine the environmental impacts related to the product's life cycle.[30,31] The International Organization for Standardization (ISO standard 14044–14044:2006) provides guidelines for the LCA modeling steps including scope and objectives, life cycle inventory (LCI) analysis, life cycle impact assessment (LCIA), and interpretation.[30,32]

Goal and scope of the study

This article examines the sustainability of the adsorbent synthesis process with a particular emphasis on its potential for large-scale industrial production. The investigation of the sustainability aspect is key for the further advancement of the developed adsorbent material for water purification applications on a large scale. The LCA method was implemented for the assessment of environmental performance of the adsorbent synthesis approach. The LCA study of adsorbent synthesis was performed using Sphera LCA for Expert software (version 10.5.1.124) and the Centrum voor Milieukunde Leiden (CML) method was opted for environmental impact information.

In this study, the gate-to-gate LCA approach encompassing the material input till product synthesis was used. Several impact indicators were calculated with the CML method including abiotic depletion, elements (ADP), abiotic depletion, fossil (ADP Fossil), acidification potential (AP), eutrophication potential (EP), freshwater aquatic ecotoxicity potential (FAETP), global warming potential (GWP 100 years), global warming potential (GWP 100 years excl biogenic), photochemical ozone creation potential (POCP), human toxicity potential (HTP), marine aquatic ecotoxicity (MAETP), ozone layer depletion potential (ODP), and terrestrial ecotoxicity potential (TETP). This study prioritizes the climate-change impact indicator among various calculated impact indicators because the climate-change impact has a significant impact on the environment. The objective of LCA is to highlight the environmental sustainability of materials through synthesis procedures.

System boundary

Fig. 2 shows the LCA boundaries which indicate all items within these boundaries were considered. This includes the chemicals and energy input and associated emission during the adsorbent synthesis process. The LCA analysis considered 1 kg of adsorbent materials as the functional unit (FU). This study explores the sustainability of adsorbent synthesis technology for the further advancement of developed adsorbent material for water purification application at large scale.

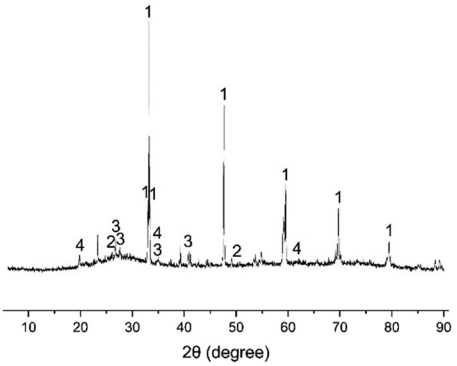

Fig. 2 XRD of the adsorbent. Compounds: (1) calcium titanium oxide, (2) silicon oxide, (3) aluminium oxide silicate, and (4) sodium aluminium silicate hydroxide hydrate.

Results and discussion

Characterization of adsorbent

XRD. XRD measurements were made to assess the incorporation of calcium titanate into the AAM framework. An XRD diffractogram of the adsorbent in presented in Fig. 3. As shown in Fig. 3, the main reflections were matched to calcium titanium oxide $Ca(TiO_3)$ (ICDD 01-081-8560) with 2θ values of 33.0, 33.2, 33.4, 47.6, 59.5, 69.7, 79.5; silicon oxide SiO_2 (ICDD 01-085-0865) 26.7, 50.2; aluminium oxide silicate Al_2O_5Si (ICDD 04-014-9725) 26.7, 27.6, 34.9, 40.7; and sodium aluminium silicate hydroxide hydrate $Al_6H_{18}Na_{0.3}O_{34}Si_8$ (ICDD 00-022-0956) 19.8, 35.0, 62.1. A typical hump for amorphous aluminosilicates can be found at 2θ values of 20–30°[33] and the five maximum intensity reflections were identified as calcium titanate.

XRF. To obtain the metal oxide ratios, the pure metakaolin-based AAM and Ca–Ti-modified AAM adsorbents were analyzed by XRF. The XRF results are presented in Table 1. Comparison between AAMs revealed that the aluminium content remained nearly constant but approximately 12% decrease in SiO_2 content was observed with Ca–Ti-modified AAM, whose TiO_2 content was 14.11%. This suggests that part of the Si in AAM's main framework was replaced by Ti, indicating the structure of the titanate-modified AAM (Adsorption and regeneration mechanism section).

DRIFTS. The DRIFTS spectrum of the adsorbent is presented in Fig. 4. Bands in 1650 and 3400 cm^{-1} correspond to O–H stretching vibrations and H–O–H bending vibrations of water

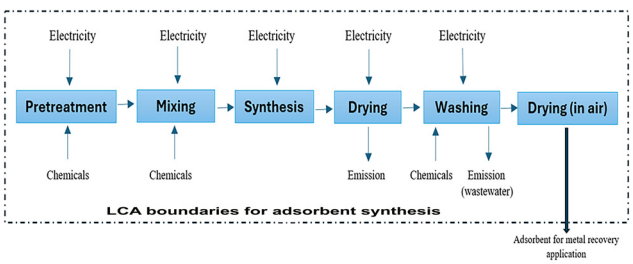

Fig. 3 LCA boundaries for the synthesis of adsorbent material.

Table 1 Adsorbent content of elements as mass % by XRF

	Al_2O_3	Al	SiO_2	Si	TiO_2	Ti	CaO	Ca	Na_2O	Na	O
Ca–Ti-modified AAM	19.01	10.06	45.15	21.10	14.11	8.46	11.86	8.48	6.10	4.52	45.03
Pure MK-based AAM	17.78	9.41	57.09	26.74	0.72	0.43	0.36	0.26	15.19	11.27	45.78

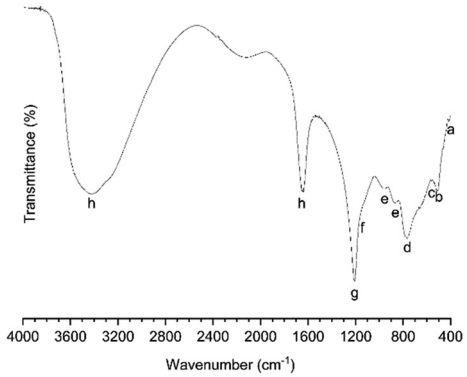

Fig. 4 DRIFTS spectrum of the adsorbent. Vibrational modes: (a) TiO2/SiO2, (b) Ti–O–Ti, (c) TiO2/SiO2, (d) Ti–O/Si–O–Al, (e) Si–O–Si/Si–O–Ti/Si–OH, (f) Si–O, (g) Ti–O and (h) Al/Si–OH⋯H2O.

molecules in Al/Si–OH⋯H_2O.[33,34] The rest of the bands from 450 to 1200 correspond to TiO_2/SiO_2, Ti–O–Ti, Ti–O, Si–O–Ti, Si–O and Ti–O vibrations.[17,35] The main bands with wavenumbers 768 cm^{-1} and 1200 cm^{-1} are Ti–O vibrations from TiO_4, followed by Si–O symmetrical stretching at 1058 cm^{-1}. The band at 768 cm^{-1} could also correspond to Si–O–Al from metakaolin.[35] Bands with wavenumbers from 866 to 954 are Si–O–Si/Si–OH bending and Si–O–Ti from condensed TiO_4 vibrations.[36] Smaller wavenumber bands from 439 cm^{-1} to 461 cm^{-1} are attributed to TiO_2/SiO_2 vibrations and Si–O–Si and Ti–O–Ti rocking.[37]

FESEM-EDS. Ca–Ti-modified AAM was characterized by FESEM-EDS. The image of the AAMs surface and the table of elements are presented in Fig. 5 and Table 2. The analysis showed that there was a large variety of different pore sizes on the surface, which was due to the preparation method. In the curing process, excess water was removed in the oven which affected the materials porosity and pore size distribution.[38] It was also noted that the main elements on the surface were silica, oxygen, aluminum, calcium, sodium and titanium. Modification with calcium titanate was done successfully, and titanium content was over 5 wt% on the surface.

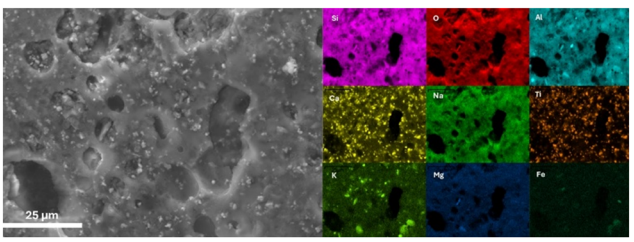

Fig. 5 FESEM-EDS image of Ca–Ti-modified AAM (25 μm).

XPS. The XPS survey of the final product is shown in Fig. 6a and Table 3. According to the "XPS knowledge view" of the Avantage software, the main peaks are Al 2p oxide with binding energy 74.4 eV; Si 2p oxide 102.6 eV; Ca $2p_{3/2}$ oxide 348.1 eV; Ti 2p oxide 456.6 eV; and O 1s 531 eV. There are also some traces of K $2p_{3/2}$ oxide and C 1s observed from the XPS survey. The Na 1s peak of 1072–1075 eV has split into two separate ones indicating the possible occurrence of Na–Si and Na–Al according to Avantage software. From the O 1s scan (Fig. 6b) and Table 3, we can conclude that aluminium oxide and silicon oxide are the main compounds, with a few condensed water molecules and no metal oxide on the surface.

Surface potential

The point of zero charge (PZC) of the material was determined to find the optimum pH range for adsorption using an acid–base potentiometric method.[39] A total of 0.2 g of adsorbent was added to a 0.1 M KCl solution for each of 11 samples, with initial pH values ranging from 2 to 12 (in increments of 1 pH unit). After 24 hours, the change in pH was measured by comparing the initial and final pH values. Results are shown in Fig. 7. It is clearly seen that the material optimum negative surface charge is approximately at the pH value of 4.5. Also from the results, the deprotonation stage between the pH values of 2 to 4.5 is noticeable. The PZC is approximately at pH 10.5.

Optimization of adsorption capacity

The optimum conditions for the adsorbent were optimized by both process flow and metal concentrations. After each test, the column was washed downstream with deionized water followed by a regeneration cycle with sodium citrate solution (0.5 M, pH 6.5). The effect of metal ion concentration and process flow was studied with closed loop configuration using column a. Single

Table 2 EDS analysis of Ca–Ti-modified AAM

Element	O	Si	Al	Ca	Ti	Na	K	Fe	Mg
Weight %	50.9	20.8	9.8	7.9	5.6	3.6	0.8	0.3	0.2

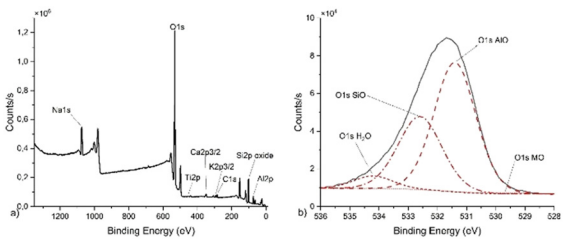

Fig. 6 XPS results: (a) survey, (b) O 1s scan.

Table 3 XPS results, binding energy (eV) and atom content (%)

	Al 2p oxide	Si 2p oxide	Na 1s		Ti 2p oxide	C 1s	Ca $2p_{3/2}$ oxide	O 1s			
			Na–Si	Na–Al				M–O	Al–O	Si–O	O H_2O
Binding energy (eV)	74.4	102.6	1072.1	1075	456.6	284.8	348.1	529.7	531.4	532.6	534.2
Atom %	9.9	19.7	3.1	5.6	0.1	2.4	0.6	0.3	34.6	20.6	3.2

metal tests were performed with direct flow configuration with 8 different metal ions and both *q*-values and adsorption efficacy were determined.

Comparing the efficacy and performance of the adsorbent used in this study to those reported in other studies is challenging due to significant variations in experimental parameters. These include differences in adsorbent form (*e.g.*, powder, foam), experimental setup, initial metal ion concentrations, contact time, pH, and whether single-metal or multimetal solutions were used. The presence of multiple metal ions introduces competitive adsorption effects, which can substantially influence adsorption capacities. For instance, Novais *et al.*[40] employed metakaolin-based AAM foams with aluminum powder as a porogen, achieving a maximum adsorption capacity (*q*-value) of 105.9 mg g^{-1} for Pb^{2+} using an 800 mg L^{-1} solution at pH 5 and a contact time of 4 hours under magnetic stirring. Andrejkovičová *et al.*[41] reported equilibrium times of 7–8 hours and a *q*-value of 24.9 mg g^{-1} for Pb^{2+} using a 250 mg L^{-1} solution and a bulk adsorbent dosage of 200 mg. Langmuir isotherm-derived maximum adsorption capacities (*q*-values) for Pb^{2+}, Cd^{2+}, Zn^{2+}, Cu^{2+}, and Cr^{3+} were 247.14, 74.36, 30.52, 44.73, and 21.84 mg g^{-1}, respectively. Notably, *q*-values exceeding 80 mg g^{-1} are rarely achieved in laboratory conditions,[42] highlighting the need for caution when comparing calculated and experimental values.

Kara *et al.*[43] conducted fixed-bed column adsorption experiments (13 mm diameter) using powdered metakaolin AAM (<150 μm) for 100 mg L^{-1} Ni^{2+} and Zn^{2+} solutions. They identified optimal flow rates of 2.0 mL min^{-1} for Zn^{2+} and 1.0 mL min^{-1} for Ni^{2+}, with corresponding optimal dosages of 3.2 g L^{-1} and 5.0 g L^{-1}. The Langmuir model yielded maximum *q*-values of 74.53 mg g^{-1} for Zn^{2+} and 42.61 mg g^{-1} for Ni^{2+}. In contrast, the present study employed significantly larger column sizes, higher flow rates, greater adsorbent dosages, and more concentrated multimetal solutions than those reported in the literature. These differences offer a new perspective on the performance and scalability of AAM-based adsorbents.

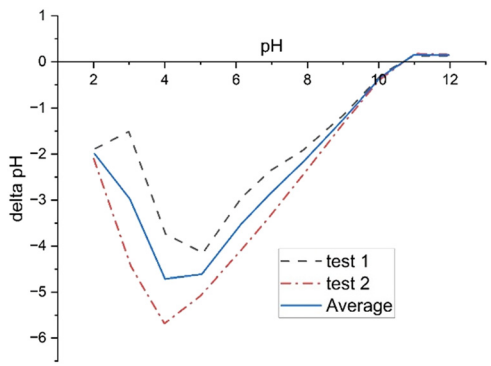

Fig. 7 Determination of surface charge of the material by acid–base titration method.

Multimetal ion adsorption experiments: concentration and flow rate

The effect of metal ion concentration of the multimetal solution was investigated with closed loop configuration using column a. The concentrations tested were 100, 250, 500, 1000 and 5000 mg L^{-1} as each metal ion concentration in the multicomponent solution. The sample volume was 1000 mL with a constant flow of 100 mL min^{-1}. The process run time was 45 min, giving a total flow through volume of 4500 mL. Samples were taken at 5, 10 and 15 minute intervals from the permeate line and finally from the sample vessel and the metal concentration were measured by AAS to determinate the *q*-values and adsorption efficiency. The result of the test is presented in Fig. 8a and b. From the results, the competition effect of different metal ions in multimetal solution can be observed clearly. Copper tends to adsorb with a higher adsorption rate than manganese and zinc. Up to 1000 mg L^{-1} the calculated *q*-value rate is linear, after which the rate is leveled. As for adsorption efficacy, the percentage is over 90% with all metals up to 250 mg L^{-1} decreasing to 59.5% for zinc and 49.7% for manganese with a

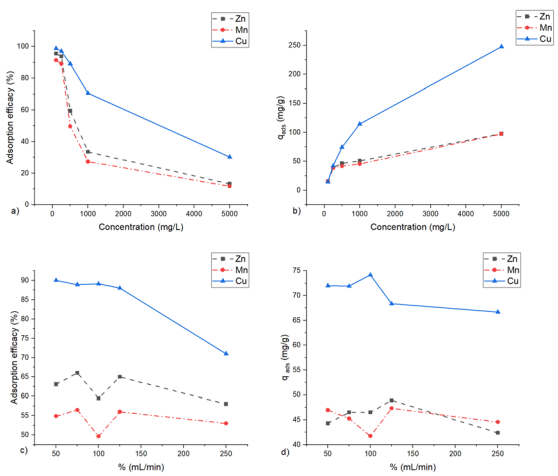

Fig. 8 The effect of concentration and flow rate on adsorption efficacy (a and c) and *q*-values (b and d). (a and b) Flow rate 100 mL min^{-1}, pH 4.5 and temperature 25 °C. (c and d) Concentration 500 mg L^{-1}, pH 4.5 and temperature 25 °C.

concentration of 500 mg L^{-1} and 33.5% for zinc and 27.3% for manganese with a concentration of 1000 mg L^{-1}. For copper the percentages were 89.1% and 70.6%. Therefore, it can be concluded that the maximum metal concentration for effective removal is approximately 500 mg L^{-1}.

For process flow rate experiments, the Me^{2+} concentration of 500 mg L^{-1} for each metal was selected from previous results and samples were taken and analyzed as previously mentioned. The flow rates tested were 50, 75, 100, 125 and 250 mL min^{-1} and the total sample volume flow through the column was kept constant at 4500 mL to keep the proportionality between tests. The results are presented in Fig. 8c and d. From the result it can be concluded that the flow rate remained nearly constant with calculated *q*-values with all flow rates. However, with calculated adsorption efficacy it can be observed that in the case of copper, the efficacy percentage decreases 17% from 88.0% to 71.0% when the flow rate increases from 125 ml min^{-1} to 250 ml L^{-1}.

Single metal ion adsorption experiment

To gain a comparison of adsorbent efficacy to other adsorbents studied from the literature, direct flow single metal solution experiments were carried out with column b. Eight different metal ions were selected: zinc, copper, manganese, nickel, cobalt, lead, cadmium and lithium. Metal concentration was kept constant at 2000 mg L^{-1} for each metal with a total sample volume of 4500 ml and the flow rate was selected as 100 ml min^{-1} from previous tests. Samples were analyzed by AAS and ICP-OES. Results are presented in Fig. 9. The order of calculated *q*-values and adsorption efficacy % was Li < Ni < Co < Zn < Mn < Cu < Cd < Pb with values from 13.4 to 66.6 mg g^{-1} for *q*-values and 21.0 to 99.6% for adsorption efficacy. This is in line with the trend from the literature.[44–47] The lower value for lithium is explained by the valency of 1 while others are multivalent. The observed order of metal ion adsorption efficacy in this study can be explained by considering the Pauling electronegativity, ionic radii, and hydration energy of the metal ions used (Table 4).[48,49] The adsorption rates showed a strong correlation with ionic radii and hydration energy except in the case of copper. Generally, ions with larger ionic radii and lower hydration energies exhibited higher adsorption extents. Minor variations among the d-block metal ions can be attributed to coordination chemistry and the complex nature of the adsorption mechanisms, which include electrostatic interactions, surface complexation, and ion exchange.

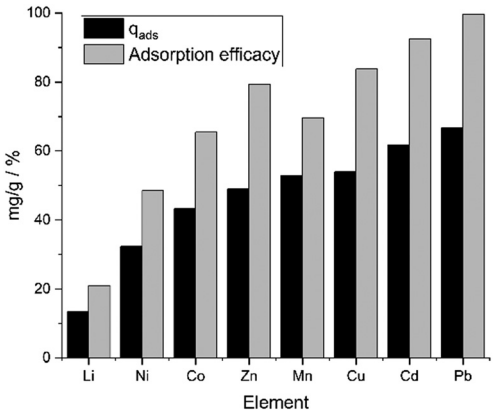

Fig. 9 *q*-Values and adsorption efficacy of single-metal tests. Metal concentrations were 2000 mg L^{-1}, flow rate was 100 mL min^{-1}, pH 4.5 and temperature was 25 °C. *q*-Values are in mg g^{-1} and efficacy in percentage. Experiments were conducted in direct flow configuration.

Optimization of regeneration efficacy

Regeneration conditions were optimized in relation to pH, concentration and contact time. The AAMs' high regeneration performance for copper was proved by conducting several adsorption–regeneration cycles, 31 in total. Cycles were conducted without any sign of material breakdown or significant decrease in adsorption capacity, which have been usually reported in the literature with other materials.[50–53]

Concentration and pH

The effect of the citrate concentration on the regeneration efficacy was studied in the range of 0.1–1 M. Range was selected by the criterion that regeneration must be efficient but still an economically sustainable solution to reduce costs and to minimize the environmental impact.[58] It was shown that with all the elements, Cu, Zn and Mn, the highest efficacy was achieved with a citric acid concentration of 0.5 M. Regeneration efficacy decreased with all metals, while the strength of the regeneration solution increased. This is most probably because the viscosity of the regeneration solution increases and for that reason the regeneration solution's ability to permeate through the AAM is decreased.[59] Results are presented in Fig. 10a.

The effect of the regeneration solution pH on the regeneration efficacy was studied in the range of 6.6–10.6. By varying the pH of the regeneration solution, it was shown that citric acid can be used under alkaline conditions (citrate form) because it does not alter the AAM structure. A study showed that by changing the pH of the regeneration solution, it was possible to alter the ratio of heavy metals removed. For instance, it was shown with copper that the highest value was achieved at the pH level of 9.6. With manganese and zinc, the optimal pH value was a bit lower, 6.6 and 7.6, respectively. For multimetal regeneration, it was noted that the optimal pH level was 6.6. This might be because zinc and manganese tend to bind in more acidic conditions than copper, which result in more competition between these heavy metal cations and eventually also the increased copper removal. Results are presented in Fig. 10b.

Adsorption–regeneration cycles

Adsorption–desorption cycles were performed in the same way during all cycles. A 500 mg L^{-1} copper solution was used as adsorbate and a total of 31 cycles were performed.

Table 4 Pauling electronegativity,[54] ionic radii[55] and hydration energy[56,57] of metal ions

Element	Li	Ni	Co	Zn	Mn	Cu	Cd	Pb
Electronegativity	0.98	1.91	1.88	1.65	1.55	1.90	1.69	2.20
Ionic radii (Å)	0.606	0.704	0.742	0.744	0.833	0.764	0.936	1.215
Hydration energy (kJ mol^{-1})	−515	−2069	−2003	−2043	−1848	−2086	−1843	−1513

Regeneration with pH-adjusted citrate therefore did not affect the mechanical durability of the AAM, which is a groundbreaking advantage compared to other regeneration chemicals, such as acetic acid.[50] During the cycles, it was noticed that the adsorption capacity showed only a negligible change. The removal % was over 95% during all cycles. This means that adsorption efficacy was affected by only 4% during 31 adsorption–regeneration cycles (not shown). In the literature, this percentage is substantially higher and for that reason only a limited number of cycles is conducted.[51–53,60] As a regeneration agent, citrate performed excellently even though some variability was seen in a couple of cycles. More importantly, adsorption efficacy was not affected much because of that, and it can be seen from the calculated adsorption and regeneration efficiencies, which are presented in Fig. 11. Adsorption was conducted at pH 4.5, concentration of 500 mg L^{-1}, flow rate of 100 mL min^{-1} and temperature of 25 °C. In regeneration, pH was 6.6, concentration 0.5 M, flow rate 50 mL min^{-1} and temperature 25 °C.

Column characterization after adsorption–regeneration cycles

The column was treated after the 31st adsorption–desorption cycle with a 1000 mg L^{-1} copper solution to investigate the vertical distribution of adsorbate inside the column without regeneration. Following the adsorption cycle, the column was flushed with deionized water to remove excess sample water, dismantled as a one piece, dried for 48 hours at 105 °C and sliced into five 2 cm sections. The sections were labelled as 1 to 5 from the bottom of the column and analysed by XRF, FESEM-EDS and DRIFTS.

The FESEM images illustrated minor decomposition of the AAM structure in sections 1 and 2 (not shown). The DRIFTS spectrum of the bottom and the top sections showed additional bands at the wavenumbers 1460, 1722, 2888 and 2956 cm^{-1} compared to the native column, which can be identified as CH_3, C═O, –C–H aldehydic and –C–H stretch from the residual regeneration chemicals used in previous cycles or from virgin olive oil which was used as a surfactant. However, the intensity of the vibration bands is greater in the top section than in the bottom one, which refers to the sodium citrate regeneration solution.

XRF data were gathered from all sections and are presented in Fig. 12. For comparison, the native adsorbent data from Table 1 are included. Si, SiO_2 and O content remained constant with all samples with a mass % of 45%, 21% and 45%, respectively. This indicates that the basic polymeric structure of silicon-based AAM is intact, although the Al_2O_3 content has decreased by 3.5% in section 1 from the native 19.01% to 15.60% and further gradually decreased from section 1 to 5, which is 9.96%. The same trend was observed with Na_2O from 6.1% to 3.16% and finally to 1.09%. The decrease in Na_2O mass % might be interpreted as due to using water in the backwashing stage in which hydrolysis of Na from the AAM structure occurs.

The opposite trend was found with TiO_2 and CaO content. With TiO_2, the relative mass % increased from the native 14.11% to the value of 15.49% in section 1, increasing steadily to the value of 22.50% in section 5. With CaO the values were 11.86%, 9.85% and 13.71%, respectively. This could be explained by TiO_2 and CaO leaching from the bottom parts of the columns during the adsorption stage, which are then adsorbed to the upper part of the column. A preferable explanation could be that during column manufacturing, when curing is performed in vertical orientation, the elemental distribution inside the column is changed. The CuO adsorbate was adsorbed highest to section

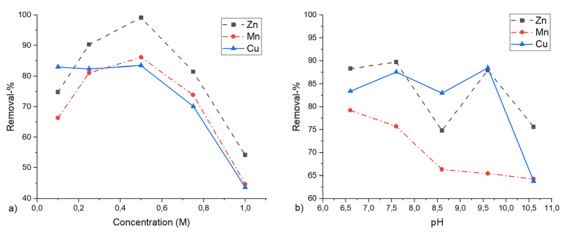

Fig. 10 The effect of the concentration (a) and pH value (b) of citrate on the regeneration for Zn, Mn and Cu. (a) pH 8.6, flow rate 50 mL min^{-1} and temperature 25 °C. (b) Citrate concentration 0.1 M, flow rate 50 mL min^{-1} and temperature 25 °C.

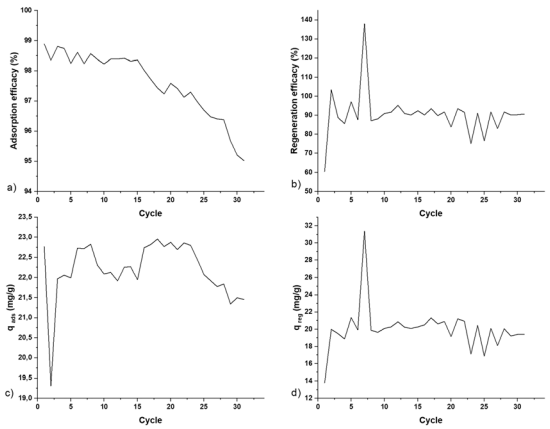

Fig. 11 Adsorption efficacy (%) (a), regeneration efficacy (%) (b), q_{ads} (mg g^{-1}) (c), and q_{reg} (mg g^{-1}) (d) for 31 consecutive adsorption–regeneration cycles of Cu.

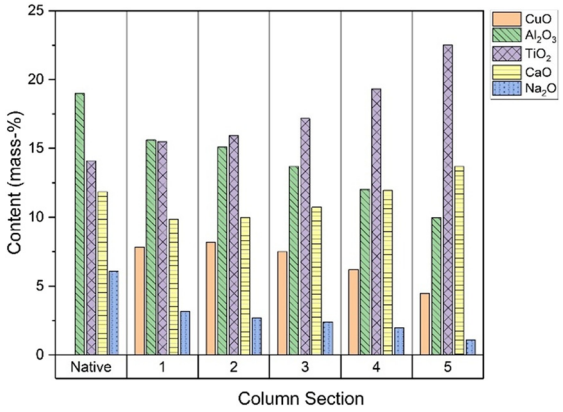

Fig. 12 Metal oxide distribution in the column after adsorption by XRF. The concentration of copper solution after 31 adsorption–desorption cycles was 1000 mg L^{-1}, pH was 4.5 and temperature 25 °C. Fresh adsorbent is labeled as native for comparison.

2 with a mass % of 8.18%, then decreased linearly to the value of 4.46% in section 5. With this AAM material and process, this would give a possibility to determine the optimum column dimensions with a certain flow to maximize the adsorption efficacy. For example, with this test, a 16 cm column height with a diameter of 4 cm should give optimum column dimensions.

Adsorption and regeneration mechanism

During the manufacturing phase, calcium titanate is added to the extremely alkaline sodium silicate activator solution. As revealed by the XRF analysis of the Ca–Ti-modified AAM (Table 1), approximately 12% of the silicon content was replaced by titanium. This substitution increases the Lewis acidity of the adsorbent and enhances the overall electronegativity of the AAM framework by introducing additional Lewis base sites. Consequently, this modification promotes acid–base coordination interactions with oxygen atoms present in the structure, thereby improving the adsorption capacity of the material.

It is assumed that the reaction generates partly calcium hydroxide and TiO_3^{2-} species, which can react with OH^- to form TiO_2, or sodium titanate (Na_2TiO_3) with reaction with Na^+ or bond straight to AAM's silicon framework during polymerization. DRIFTS data suggest the latest option of these three; however, XRD also proposes unreacted calcium titanium oxide. The proposed structure of the adsorbent is illustrated in Fig. 13.

The adsorption mechanism of metal cations is usually a two-stage process.[17] Partial hydrolysis takes place in water solutions and the surface of the adsorbent becomes negatively charged, and after pre-regeneration of the AAM with sodium citrate solution, the excess sodium is attached to the negatively charged AAM (Fig. 13). In the adsorption phase, Na^+ is replaced by adsorbate solution metal cations, depending on the charge of the cation as presented in Fig. 14. In Fig. 14, the possible adsorption sites are (1) direct

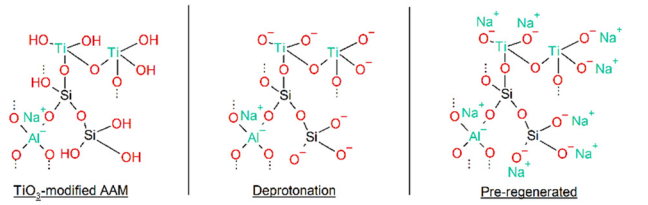

Fig. 13 Proposed structure of titanate-modified AAM, structure after deprotonation and when pre-regenerated with sodium citrate solution before experiments. The figure illustrates the continuum of the basic AAM framework.

ion exchange with Na^+ attached to the aluminium, (2) ion exchange with two Na^+ of the TiO_2 group, (3) ion exchange with two Na^+ attached to TiO–SiO groups and (4) ion exchange with two Na^+ of the SiO_2 group. Fig. 14 illustrates the continuum of the basic AAM framework.

Regeneration was performed using sodium citrate solution instead of the commonly utilized acetic acid and sodium chloride solutions, but regeneration with acetic acid, with copper for example, it can form undesirable copper acetate and due to the acidity of the solution it may deconstruct the AAM framework. Sodium citrate is considered as a triprotic acid and can be in different forms according to pH due to the number of negatively charged carboxylic groups, such as mono-, di- and trisodium citrate, with pK_α values of 3.13, 4.76 and 6.40, respectively.[61] However, some studies propose the fourth dissociation constant at a pK_α value of 13.0, which is related to deprotonation of the –OH group attached to the central carbon. In this paper, the pH range of the regeneration test was 6 to 11, in which di- and trisodium citrate species are present, with trisodium citrate becoming dominant after a pH value of 6.4.

The regeneration mechanism with di- and trisodium citrate species is presented in Fig. 15. In Fig. 15, the proposed different regeneration mechanisms are (1) adsorbed Me^{2+} ion exchange with di- and trisodium citrate forming a linkage between these two forms, (2) ion exchange with trisodium citrate, (3) ion exchange with disodium citrate

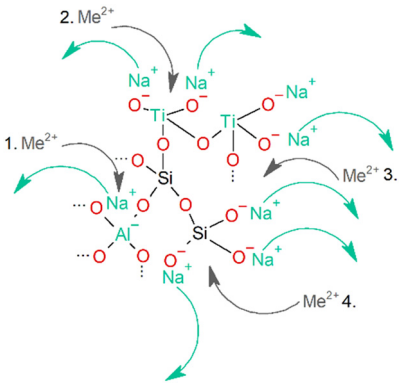

Fig. 14 Possible adsorption mechanism of Me^{2+} to titanate-modified AAM.

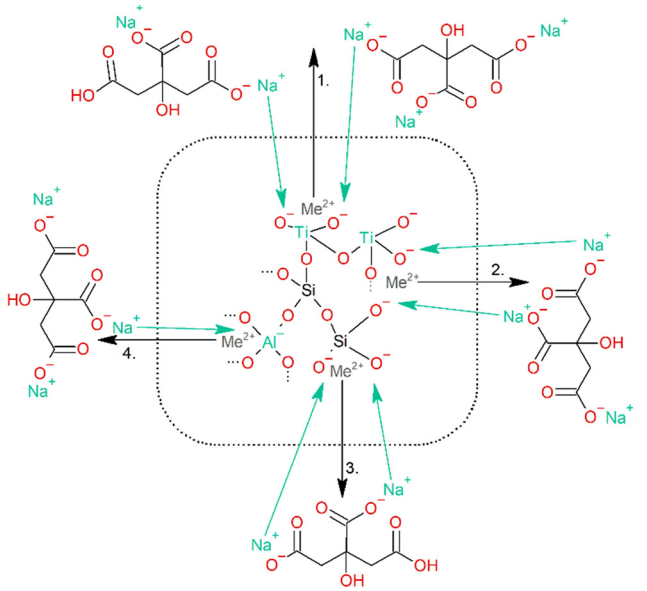

Fig. 15 Possible regeneration mechanism of Me^{2+} with di- and trisodium citrate species.

and (4) ion exchange of Me^{2+} AAM's aluminium. Also, Fig. 15 illustrates the continuum of the basic AAM framework.

LCA study for adsorbent synthesis

This study employs gate-to-gate LCA to highlight the environmental impact of adsorbent preparation. The LCA study showed that the major cause of climate impact was kaolin calcination into metakaolin, utilization of NaOH during adsorbent synthesis, electricity/energy input and wastewater generation during the production of 1 kg adsorbent, which caused significant emissions. In this study, the environmental impact categories were found to be as follows: ADP (9.73 e^{-6} kg SB eq.), ADP fossil (22.009 kg SB eq.), AP (5.46 e^{-3} kg SO_2 eq.), EP (6.6 × 10^{-4} kg phosphate eq.), FAETP (0.011 kg DCB eq.), GWP 100 years (2.01 kg CO_2 eq.), GWP 100 years excl biogenic (2.002 kg CO_2 eq.), HTP (0.209 kg DCB eq.), MAETP (1364.48 kg DCB eq.), ODP (1.77 × 10^{-10} kg R11 eq.), POCP (5.42 × 10^{-4} kg ethene eq.), TETP (4.67 × 10^{-3} kg DCB eq.). The GWP was noted to be 2.01 kg CO_2 eq. for producing 1 kg of adsorbent. When the GWP in this study was compared to that of other available adsorbents such as granulated activated carbon, nanomaterials, zeolite-based,[62–66] the result was quite comparable with the other adsorbents. However, due to different synthesis methodologies, system boundaries, and different scenarios it is quite challenging to have an exact comparison with other studies.

Conclusions

A novel Ca–Ti-modified alkali-activated material (AAM) adsorbent was successfully synthesized and characterized. Adsorption experiments were conducted using both single-metal and multimetal solutions, with sodium citrate employed as a regeneration chemical. The key findings are summarized as follows.

(a) For adsorption performance, in single metal-experiments, the calculated adsorption capacities (q-values) and removal efficiencies followed the order Li < Ni < Co < Zn < Mn < Cu < Cd < Pb, with q-values ranging from 13.4 to 66.6 mg g^{-1} and removal efficiencies from 21.0% to 99.6%. In multimetal experiments involving Zn^{2+}, Mn^{2+}, and Cu^{2+} at five different concentrations and flow rates, the maximum concentration used was 500 mg L^{-1} per metal ion. The optimal flow rate was determined to be 125 mL min^{-1} based on both q-values and removal efficiency, using a column of 4 cm diameter and 10 cm height.

(b) For regeneration optimization, a novel regeneration chemical based on citric acid was developed, marking its first reported use with AAMs. In single-metal regeneration, optimal pH values were 9.6 (Cu), 6.6 (Mn), and 7.6 (Zn). For multimetal regeneration, the optimal pH was 6.6, and the best-performing sodium citrate concentration was 0.5 M.

(c) For long-term adsorption and regeneration performance, a previously unreported series of 31 consecutive adsorption–regeneration cycles was conducted using a 500 mg L^{-1} Cu^{2+} solution. The removal efficiency remained consistently above 95% throughout all cycles, indicating that adsorption efficacy was reduced by only 4%. Regeneration performance also remained stable, with only minor fluctuations observed across cycles.

(d) Column characterization after 31 cycles revealed that CuO adsorbate was most concentrated in section 2, with a mass percentage of 8.18%, gradually decreasing to 4.46% in section 5. This distribution suggests an optimal column size ratio of 1 : 4 (diameter : height) under the tested conditions. Additionally, uneven elemental composition within the column indicates that alternative drying methods, such as rotational horizontal drying, may be more suitable than the vertical stationary drying used in this study for future column fabrication.

(e) Mechanistic insights were presented based on pH optimization results. For single-metal solutions, the trisodium citrate form is favored (pK_α > 6.6), enhancing regeneration efficiency. In multimetal systems, the optimal pH of 6.6 corresponds to a mixture of di- and trisodium citrate forms in approximately equal molar ratios (50 : 50). Both direct metal–citrate binding and inter-citrate linking are proposed as contributing mechanisms.

(f) The LCA revealed that the primary contributors to climate impact were kaolin calcination (to produce metakaolin), NaOH usage during synthesis, energy consumption, and wastewater generation. The global warming potential (GWP) was calculated to be 2.01 kg CO_2 eq. per kg of adsorbent, which is comparable to values reported for conventional adsorbents such as activated carbon.

In summary, the results demonstrate the strong potential of Ca–Ti-modified AAM adsorbents for scalable, sustainable metal ion recovery. The system's high adsorption and

regeneration performance, combined with promising LCA metrics, supports its applicability in real-world scenarios. Future studies should focus on scaling up column dimensions and testing with actual mining wastewater to simulate commercial processes more accurately.

Author contributions

M. K. and A. P. were responsible for the investigation, conceptualization, writing the original draft, formal analysis, visualization, and funding acquisition. H. R. was responsible for writing, reviewing and editing, and supervision (M. K. and A. P.). T. H. was responsible for formal analysis and writing, reviewing, and editing. S. T. was responsible for writing, reviewing, and editing, supervision (M. K. and A. P.), and administration. U. L. was responsible for funding, supervision (M. K. and A. P.), writing, reviewing and editing.

Conflicts of interest

There are no conflicts to declare.

Data availability

All data is reported in this paper.

Acknowledgements

The authors acknowledge Business Finland, CAAMA project (Grant no. 1840/31/2023). The authors also would like to thank the Finnish Natural Resources Research Foundation (Grant numbers 20230035 and 20240018) and Maa-ja vesitekniikan tuki foundation (Grant number 44053) for their financial support. The authors would also like to thank laboratory staff Juhani Väisänen, Mikko Häkkinen and Markus Väyrynen for analyzing the samples.

References

1 V. Coman, B. Robotin and P. Ilea, *Resour., Conserv. Recycl.*, 2013, **73**, 229–238.
2 S. Lata, P. K. Singh and S. R. Samadder, *Int. J. Environ. Sci. Technol.*, 2015, **12**, 1461–1478.
3 X. Wu, S. J. Cobbina, G. Mao, H. Xu, Z. Zhang and L. Yang, *Environ. Sci. Pollut. Res.*, 2016, **23**, 8244–8259.
4 T. H. Tan, K. H. Mo, T. C. Ling and S. H. Lai, *Environ. Technol. Innovation*, 2020, **18**, 100684.
5 S. Sireesha, U. Upadhyay and I. Sreedhar, *Biomass Convers. Biorefin.*, 2022, DOI: **10.1007/s13399-021-02186-2**.
6 V. Singh, G. Ahmed, S. Vedika, P. Kumar, S. K. Chaturvedi, S. N. Rai, E. Vamanu and A. Kumar, *Sci. Rep.*, 2024, **14**, 7595.
7 M. P. Christophliemk, A. T. Pikkarainen, A. Heponiemi, S. Tuomikoski, H. Runtti, T. Hu, A. M. Kantola and U. Lassi, *Appl. Clay Sci.*, 2022, **230**, 106697.
8 M. Manninen, T. Kangas, T. Hu, T. Varila, U. Lassi and H. Runtti, *Environ. Technol.*, 2023, 1–73.
9 E. Sundhararasu, S. Tuomikoski, H. Runtti, T. Hu, T. Varila, T. Kangas and U. Lassi, *ChemEngineering*, 2021, **5**(1), DOI: **10.3390/chemengineering5010013**.
10 E. Svobodová, Z. Tišler, K. Peroutková, K. Strejcová, J. Abrham, J. Šimek, Z. Gholami and M. Vakili, *Molecules*, 2024, **29**(10), DOI: **10.3390/molecules29102357**.
11 S. Yan, X. Feng, K. Huang, X. Ren, Y. Zhao and P. Xing, *Int. J. Appl. Ceram. Technol.*, 2023, **20**, 1591–1605.
12 N. Kabir, J. Finnilä, J. Laukkanen and T. Luukkonen, *Chem. Eng. Res. Des.*, 2024, **212**, 485–492.
13 Y. D. Noh, S. Komarneni and K. J. D. MacKenzie, *Sep. Purif. Technol.*, 2012, **95**, 222–226.
14 R. Bai, M. T. Navarro, Y. Song, T. Zhang, Y. Zou, Z. Feng, P. Zhang, A. Corma and J. Yu, *Chem. Sci.*, 2020, **11**, 12341–12349.
15 J. C. Almeida, C. Sousa, D. S. Tavares, J. Pinto, B. Henriques, Z. Lin, J. Rocha and E. Pereira, *Environ. Sci. Pollut. Res.*, 2024, **31**, 28856–28869.
16 D. M. Poojary, R. A. Cahill and A. Clearfield, *Chem. Mater.*, 1994, **6**, 2364–2368.
17 I. Perovskiy, N. Y. Yanicheva, V. V. Stalyugin, T. L. Panikorovskii and A. A. Golov, *Microporous Mesoporous Mater.*, 2021, **311**, 110716.
18 A. Tripathi, D. G. Medvedev, J. Delgado and A. Clearfield, *J. Solid State Chem.*, 2004, **177**, 2903–2915.
19 A. K. Adepu, V. Katta and V. Narayanan, *New J. Chem.*, 2017, **41**, 2498–2504.
20 D. Yang, H. Liu, Z. Zheng, S. Sarina and H. Zhu, *Nanoscale*, 2013, **5**, 2232–2242.
21 T. Tratnjek, X. Deschanels, A. Hertz, C. Rey and J. Causse, *J. Hazard. Mater.*, 2022, **440**, 129755.
22 X. Zhao, P. Du, Z. Cai, T. Wang, J. Fu and W. Liu, *Environ. Pollut.*, 2018, **232**, 580–590.
23 S. Chitra, S. Viswanathan, S. V. S. Rao and P. K. Sinha, *J. Radioanal. Nucl. Chem.*, 2011, **287**, 955–960.
24 B. N. Alum, *INOSR Appl. Sci.*, 2024, **12**, 51–56.
25 İ. Kara, D. Yilmazer and S. T. Akar, *Appl. Clay Sci.*, 2017, **139**, 54–63.
26 E. Repo, J. K. Warchoł, L. J. Westholm and M. Sillanpää, *J. Ind. Eng. Chem.*, 2015, **27**, 115–125.
27 H. Patel, *Appl. Water Sci.*, 2019, **9**, 45.
28 Y. Liao, W. Ge, M. Liu, W. Bi, C. Jin and D. D. Y. Chen, *Int. J. Biol. Macromol.*, 2024, **260**, 129677.
29 A. C. J. Abraham, *Biotechnol. Lett.*, 2019, **41**, 319–333.
30 C. A. Grande, R. Blom, A. Spjelkavik, V. Moreau and J. Payet, *Sustainable Mater. Technol.*, 2017, **14**, 11–18.
31 H. U. Escobar-Hernandez, Y. Quan, M. I. Papadaki and Q. Wang, *ACS Sustainable Chem. Eng.*, 2023, **11**, 4219–4225.
32 G. H. Patel, M. Horttanainen, M. Kokko, H. C. Yörüklü and J. Havukainen, *Energy*, 2025, **320**, 135244.
33 V. F. F. Barbosa, K. J. D. MacKenzie and C. Thaumaturgo, *Int. J. Inorg. Mater.*, 2000, **2**, 309–317.
34 H. Rahier, W. Simons, B. Van Mele and M. B. Ans, *J. Mater. Sci.*, 1997, **32**, 2237–2247.
35 A. Tironi, M. Trezza, E. Irassar and A. N. Scian, *Procedia Mater. Sci.*, 2012, **1**, 343–350.

36 A. Damin, G. Ricchiardi, S. Bordiga, A. Zecchina, F. Ricci, G. Spanò and C. Lamberti, *Stud. Surf. Sci. Catal.*, 2001, **140**, 195–208.
37 M. Chellappa, B. Thejaswini and U. Vijayalakshmi, *IET Nanobiotechnol.*, 2017, **11**, 77–82.
38 M. P. Christophliemk, A. T. Pikkarainen, A. Heponiemi, S. Tuomikoski, H. Runtti, T. Hu, A. M. Kantola and U. Lassi, *Appl. Clay Sci.*, 2022, **230**, 106697.
39 M. K. Miyittah, F. W. Tsyawo, K. K. Kumah, C. D. Stanley and J. E. Rechcigl, *Commun. Soil Sci. Plant Anal.*, 2016, **47**, 101–111.
40 R. M. Novais, J. Carvalheiras, M. P. Seabra, R. C. Pullar and J. A. Labrincha, *J. Environ. Manage.*, 2020, **272**, 111049.
41 S. Andrejkovičová, A. Sudagar, J. Rocha, C. Patinha, W. Hajjaji, E. F. Da Silva, A. Velosa and F. Rocha, *Appl. Clay Sci.*, 2016, **126**, 141–152.
42 T. Luukkonen, *Alkali-activated materials in environmental technology applications*, Woodhead Publishing Series in Civil and Structural Engineering, 2022.
43 İ. Kara, D. Yilmazer and S. T. Akar, *Appl. Clay Sci.*, 2017, **139**, 54–63.
44 B. Buhani, N. Narsito, N. Nuryono, E. Sri Kunarti and S. Suharso, *Desalin. Water Treat.*, 2015, **55**, 1240–1252.
45 F. Cherono, N. Mburu and B. Kakoi, *Heliyon*, 2021, **7**, e08254.
46 S. Tuomikoski, H. Runtti, H. Romar, U. Lassi and T. Kangas, *Water Environ. Res.*, 2021, **93**, 1303–1314.
47 P. Nhambe, B. Patel, T. Y. Leswifi, J. Abdulsalam and N. Gardee, *Int. J. Environ. Sci. Technol.*, 2024, 1–16.
48 X. Fan, H. Liu, E. Anang, D. Ren, D. Gennaro, B. Liguori, A. Colella and D. Caputo, *Materials*, 2021, **14**, 4066.
49 L. de Castro-Alves, S. Yáñez-Vilar, M. A. González-Goméz, P. Garcia-Acevedo, Á. Arnosa-Prieto, Y. Piñeiro-Redondo and J. Rivas, *Microporous Mesoporous Mater.*, 2024, **374**, 113159.
50 M. Manninen, T. Kangas, T. Hu, T. Varila, U. Lassi and H. Runtti, *Environ. Technol.*, 2024, **45**, 2519–2530.
51 X. Shen, G. Qiu, C. Yue, M. Guo and M. Zhang, *Environ. Sci. Pollut. Res.*, 2017, **24**, 21829–21835.
52 S. Sireesha, U. Upadhyay and I. Sreedhar, *Biomass Convers. Biorefin.*, 2022, DOI: **10.1007/s13399-021-02186-2**.
53 S. Sulaiman, R. S. Azis, I. Ismail, H. C. Man, K. F. M. Yusof, M. U. Abba and K. K. Katibi, *Nanoscale Res. Lett.*, 2021, **16**, 168.
54 D. F. Shriver, P. W. Atkins and C. H. Langford, *Inorganic Chemistry*, Oxford University Press, 1992.
55 F. C. Hawthorne and O. C. Gagné, *Acta Crystallogr., Sect. B: Struct. Sci., Cryst. Eng. Mater.*, 2024, **80**, 326–339.
56 K. P. Kepp, *J. Phys. Chem. A*, 2018, **122**, 2025.
57 A. G. Volkov, S. Paula and D. W. Deamer, *Bioelectrochem. Bioenerg.*, 1997, **42**, 153–160.
58 S. Lata, P. K. Singh and S. R. Samadder, *Int. J. Environ. Sci. Technol.*, 2015, **12**, 1461–1478.
59 A. Valverde and I. M. Griffiths, *Discover Chem. Eng.*, 2024, **4**, 27.
60 E. Sundhararasu, S. Tuomikoski, H. Runtti, T. Hu, T. Varila, T. Kangas and U. Lassi, *ChemEngineering*, 2021, **5**(1), DOI: **10.3390/chemengineering5010013**.
61 S. Krukowski, M. Karasiewicz and W. Kolodziejski, *J. Food Drug Anal.*, 2017, **25**, 717–722.
62 J. Saleem, F. Tahir, M. Zubair Khalid Baig and G. McKay, *Mater. Today: Proc.*, 2024, DOI: **10.1016/J.MATPR.2024.05.146**.
63 M. N. Garcia Gonzalez, R. Quiroga-Flores and P. Börjesson, *Clean. Environ. Syst.*, 2022, **4**, 100071.
64 C. S. Gómez-Navarro, W. M. Warren-Vega, J. C. Serna-Carrizales, A. I. Zárate-Guzmán, R. Ocampo-Pérez, F. Carrasco-Marín, V. H. Collins-Martínez, J. Niembro-García and L. A. Romero-Cano, *Materials*, 2023, **16**, 8.
65 H. U. Escobar-Hernandez, Y. Quan, M. I. Papadaki and Q. Wang, *ACS Sustainable Chem. Eng.*, 2023, **11**, 4219–4225.
66 M. H. Kim, I. T. Jeong, S. B. Park and J. W. Kim, *Environ. Eng. Res.*, 2019, **24**, 117–126.